

A Novel LVRT Control Strategy for Modular Multilevel Matrix Converter based High-Power Wind Energy Conversion Systems

Matías Díaz &
Roberto Cárdenas
Electrical Engineering Department
University of Chile
Santiago, Chile.
matias.diaz@ing.uchile.cl
rcd@ieee.org

Mauricio Espinoza B.
School of Electrical
Engineering
University of Costa Rica
San José, Costa Rica.
mespinoza@eie.ucr.ac.cr

Andrés Mora
Electrical Engineering
Department
Universidad Técnica Federico
Santa María
Valparaíso, Chile
andres.mora@usm.cl

Félix Rojas
Electrical Engineering
Department
Technical University of
Munich, Germany.
felix.rojas@tum.de

Abstract— The trend of multimegawatt wind turbines has positioning multilevel converters as a promising solution for high-power Wind Energy Conversion Systems (WECSs). Furthermore, due to the high penetration of wind energy into the electrical network, some rather strict grid regulations have been development in case of fault into the grid power. Mainly, grid codes set Low Voltage Ride Through (LVRT) requirements for grid connected WECS. In this scenario, this paper presents a novel modelation and control strategy to fulfil Low Voltage Ride Through requirements using a Modular Multilevel Matrix Converter for interfacing a high power wind turbine.

Keywords—Low Voltage Ride Through, Wind Turbine, Modular Multilevel Matrix Converter.

I. INTRODUCTION

The installed wind power has until 2013 a cumulative worldwide installation level of 318 MW, positioning wind power as an important and decisive energy source in some areas of the world as China, USA and Europe. For example, the European Union installed 12-GW through 2013, with countries as Denmark with a wind power penetration over 30% [1].

In this scenario, the European Wind Energy Association strategy for the next ten years is to become wind industry in the most competitive energy source by 2020 onshore and offshore by 2030, stating that wind power would be “capable of contributing up to 20% of EU electricity by 2020, 30% by 2030 and 50% by 2050”. Therefore, significant research and industrial efforts have to be done to bridge the gap between the 5% of the European electricity demand (currently supplied by wind energy) and the expected 20% of electricity demand in 2020, 30% by 2030 and 50% by 2050 [2].

An important part of the required future installed wind power will be offshore based, not only due to the higher wind-energy potential but also because the environmental impacts of onshore wind farms are higher. Going offshore implies several technology developments, mainly regarding reliability,

efficiency and upscaling. Moreover, the size and weight of components is extremely important, considering that extremely expensive platforms must support the total weight of the WECS. The cost structure of offshore WECS could be reduced in high power wind turbines, reason why upscaling has become in the focus of modern wind energy application and research.

In fact, the largest manufacturers of wind turbines in the world have been upscaling wind turbine dimensions for the reason mentioned above. As is depicted in Fig. 1, theoretical 20-MW wind turbine with a rotor diameter of 250 m could be feasible [2].

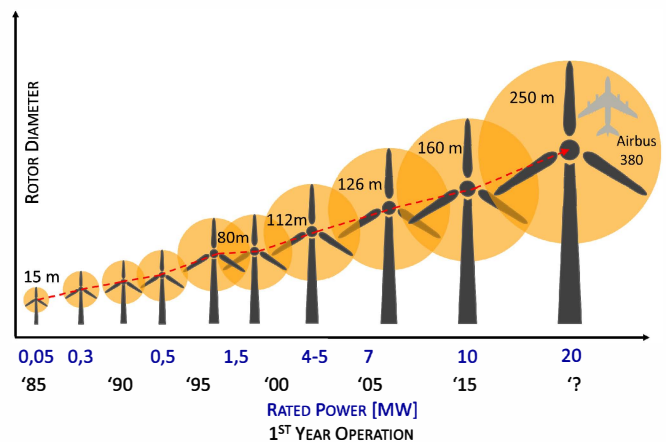


Fig. 1: Wind Turbines Rated Power increasing.

Most of present WECSs are based on low voltage two level voltage-source power converters. The use of this technology is not the best option for high-power wind turbines due to the high currents required and the fault sensibility of the converter. For example, from 1600 A required for a 2-MW system, the current will increase to 8810 A for a 10-MW system. Because of this large current value, the diameter of the cables used to connect the converter to the power transformer has to be largely increased. Large current transfer results in big rated power cables going down through the tower (for horizontal axis wind turbines), with important losses and voltage drops. Paralleling

the cables reduces the loss but increases cost because high current cables are expensive. A step-up transformer located inside the nacelle could avoid some of these disadvantages, but makes the system bulky and heavy.

Consequently, medium or high voltage power electronic converters (e.g. multilevel converters) are well suited for large wind turbines. These topologies are able to reduce the current level into the system by increasing the voltage rating, which implies costs saving due to cable cost and minimization of losses. Moreover, multilevel converters are more robust than that the traditional two level topologies in case of failures of its components.

Modular Multilevel Converters (MMC) are relatively new converter topology, with full modularity and easy extensibility to reach high voltage – power levels [3], [4]. Furthermore, this topology has good power density, does not require transformers with multiple secondary systems –as other topologies- and has high reliability. Therefore, this paper is focused on the novel application of a Direct MMC configuration –best known as Modular Multilevel Matrix Converter or M3C– to control a High Power WECS, as is shown in Fig. 2.

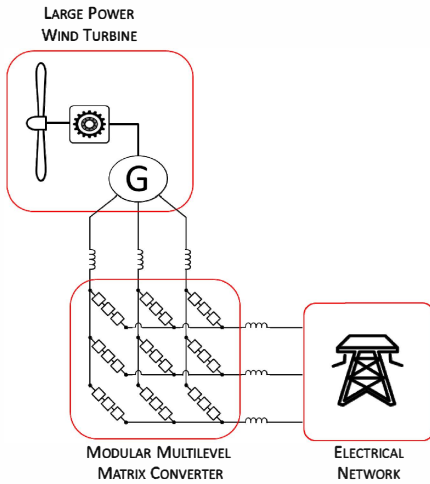


Fig. 2: Intended configuration of study: M3C interfacing very high power WECSs with the electrical network.

II. M3C OVERVIEW

The Modular Multilevel Matrix Converter was proposed in 2001 for wind applications [5]. Control principles based on space vector modulation were presented in [6] and [7]. In these papers, the branches of the converter do not have inductors and each branch is controlled as a voltage source based on space vector modulation. However, this method is not suitable for M3C with a high number of cells per arm because of the high number of possible space vectors.

In Fig. 3 the topology of a M3C is illustrated. The M3C consist of 9 branches connecting the phases of the input system ($a - b - c$), to the phases of the output system ($r - s - t$). As is presented in Fig. 3(b) and Fig. 3(c), these branches are the series connection of n Full H-Bridge based cells and an inductor.

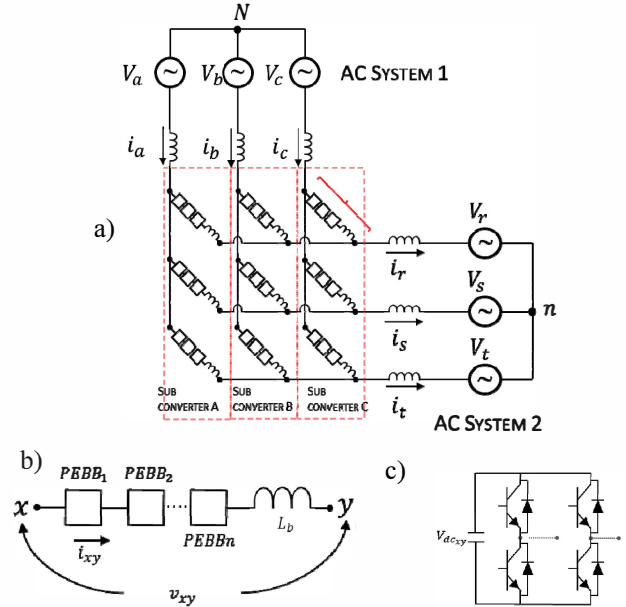


Fig. 3: Modular Multilevel Matrix Converter Topology. (a) Whole converter. (b) M3C Branch composition. (c) M3C Cells.

The switching frequency and levels of the branch voltage depend on the numbers of cells, which lead to low harmonic distortion and small voltage steps when high number of cells is considered.

Cell dc capacitor voltages can charge-discharge during normal operation of the converter because they are not regulated by external power sources. Thereby, the average value of the dc capacitor voltage has to be controlled with low ripple and zero power mean value during steady state [8], [9], [10].

To analyse the energy balancing of the M3C a single branch as the presented in Fig. 3(c) could be used. Neglecting internal losses, the energy stored in a cell is the integral of the power at its terminals. Analogously, the energy variation of a branch with n cells is proportional to the capacitor voltage ripple [8]. Thus, the capacitor voltage ripple can be determined using the branch power:

$$W_{xy} = \int P_{xy} dt = \frac{1}{2} C v_c^2 \quad (1)$$

Where: $x \in \{a - b - c\}$, $y \in \{r - s - t\}$, v_{xy} correspond to the branch terminal voltage and i_{xy} is the current flowing through the branch. The branch terminal voltage can be expressed as the difference between the phase voltages of the input/output connected by the branch, as follow:

$$v_{xy} = v_x - v_y \quad (2)$$

The branch current is composed of 1/3 of the x phase input current and 1/3 of the y phase output current. Therefore, the instantaneous branch power yields:

$$p_{xy} = (v_x - v_y) \left(\frac{i_x}{3} - \frac{i_y}{3} \right) = \frac{1}{3} (v_x i_x + v_y i_y - v_y i_x - v_x i_y) \quad (3)$$

$$p_{xy} = \frac{1}{3}(P_x(1 + \cos(2\omega_x t + \dots)) + P_y(1 + \cos(2\omega_y t + \dots)) - v_y i_x - v_x i_y) \quad (4)$$

Analysing (4) it is possible to conclude that the branch power has the following components:

- Two dc components.
- Double frequency components oscillating at $2\omega_x$ and $2\omega_y$.
- Oscillating power components of frequencies $\omega_x \pm \omega_y$.

The dc components cancel each other when the input-output is balanced [8]. Moreover, the energy associate to the sinusoidal components of (4) has a peak amplitude which is inversely proportional to the frequency ($2\omega_x$, $2\omega_y$, $\omega_x \pm \omega_y$) and directly proportional to the magnitude of the power. Consequently, there are two conditions where the energy of the branch could be problematic to control. The first one is when the frequencies of one of the phases connected by a branch is near to zero ($2\omega_x$ or $2\omega_y \approx 0$). The other condition is when the input and output frequencies are equal ($\omega_x - \omega_y \approx 0$). Therefore, for a M3C driving a high power machine, the difficult operation zones are when the machine is operating at low speed or starting, and when the machine is fed with a signal of frequency near or equal to the grid.

III. PROPOSED MODELATION FOR THE M3C

In recent literature, mathematical modelations of the M3C have been reported in [10], [11], [12] and [13]. In those papers, the basic approach is to use a so-called double $\alpha\beta 0$ transformation. The main procedure starts applying Kirchhoff's Voltage Law to Fig. 3(a) as follow:

$$V_{sx} = V_{xy} + L \frac{d}{dt} I_{xy} + V_{gy} + v_{Nn} \quad (5)$$

Then, (5) is pre-multiplied by $[C_{\alpha\beta 0}]$ and post-multiplied by $[C_{\alpha\beta 0}]^t$:

$$C_{\alpha\beta 0} V_{sx} C_{\alpha\beta 0}^t = C_{\alpha\beta 0} (V_{xy} + L \frac{d}{dt} I_{xy} + V_{gy} + v_{Nn}) C_{\alpha\beta 0}^t \quad (6)$$

$$\sqrt{3} \begin{bmatrix} 0 & 0 & 0 \\ 0 & 0 & 0 \\ v_{s\alpha} & v_{s\beta} & 0 \end{bmatrix} = \begin{bmatrix} v_{\alpha\alpha} & v_{\beta 0} & v_{0\alpha} \\ v_{\alpha\beta} & v_{\beta\beta} & v_{0\beta} \\ v_{\alpha 0} & v_{\beta 0} & v_{00} \end{bmatrix} + L \frac{d}{dt} \begin{bmatrix} i_{\alpha\alpha} & i_{\beta\alpha} & i_{0\alpha} \\ i_{\alpha\beta} & i_{\beta\beta} & i_{0\beta} \\ i_{\alpha 0} & i_{\beta 0} & i_{00} \end{bmatrix} + \sqrt{3} \begin{bmatrix} 0 & 0 & v_{g\alpha} \\ 0 & 0 & v_{g\beta} \\ 0 & 0 & 0 \end{bmatrix} + \begin{bmatrix} 0 & 0 & 0 \\ 0 & 0 & 0 \\ 0 & 0 & 3v_{Nn} \end{bmatrix} \quad (7)$$

where:

$$C_{\alpha\beta 0} = \begin{bmatrix} 1 & -1/2 & -1/2 \\ 0 & \sqrt{3}/2 & -\sqrt{3}/2 \\ 1/3 & 1/3 & 1/3 \end{bmatrix} \quad (8)$$

According with [11] and [12], the transformation presented above yields to a decoupled model of the M3C, which enables the full use of the branch currents as degrees of freedom. This transformation provides a clear definition of the circulating currents among the subconverters. Furthermore, independent

models for the input, converter and output are obtained in terms of the branch currents.

A. Proposed Modelation

The proposed modelation is based in [10], [11] and [12], but attempts to be an alternative more intuitive and with electrical meaning. In this case, the $\alpha\beta\gamma$ transformation is also applied. In a first step, the input system ($a - b - c$) is transformed to $\alpha\beta\gamma$ as is shown in Fig. 4.

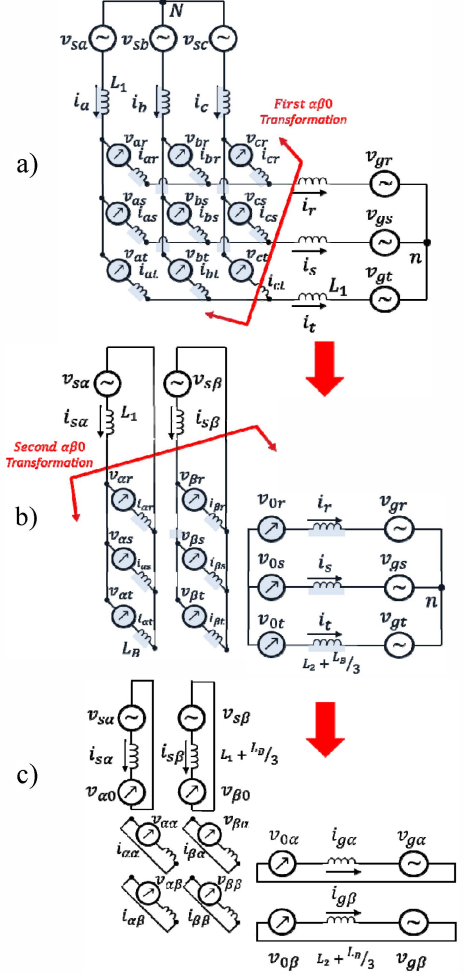


Fig.4: Proposed Modelation of the M3C.

The second step consist in apply (8) to the output system ($r - s - t$). As can be easily observed in Fig.4, the zero sequence component of v_{ay} , v_{by} , and v_{cy} correspond to the equivalent circuit that the output sees from the converter. Analogously, the zero sequence component of v_{xr} , v_{xs} , and v_{xt} can be obtained using the equivalent circuit that the input sees from the converter. Is important to note that the current between points N and n is zero because no path is considered.

Analysing Fig. 4(c), it is possible to write the following equations, which represent a decoupled model for the input, converter and output of the M3C.

$$\begin{bmatrix} v_{s\alpha} \\ v_{s\beta} \end{bmatrix} = \begin{bmatrix} v_{\alpha 0} \\ v_{\beta 0} \end{bmatrix} + (L_1 + L_B/3) \frac{d}{dt} \begin{bmatrix} i_{s\alpha} \\ i_{s\beta} \end{bmatrix} \quad (9)$$

$$\begin{bmatrix} v_{g\alpha} \\ v_{g\beta} \end{bmatrix} = \begin{bmatrix} v_{0\alpha} \\ v_{0\beta} \end{bmatrix} + (L_2 + L_B/3) \frac{d}{dt} \begin{bmatrix} i_{g\alpha} \\ i_{g\beta} \end{bmatrix} \quad (10)$$

$$\begin{bmatrix} v_{\alpha\alpha} & v_{\beta\alpha} \\ v_{\alpha\beta} & v_{\beta\beta} \end{bmatrix} = -L_B \frac{d}{dt} \begin{bmatrix} i_{\alpha\alpha} & i_{\beta\alpha} \\ i_{\alpha\beta} & i_{\beta\beta} \end{bmatrix} \quad (11)$$

IV. GRID INTEGRATION REQUIREMENTS FOR WECS

In order to ensure continuity and security of the interconnection of WECS to generation and transmission systems, stringent grid codes have been enforced in several countries, where renewable energies have a considerable impact on the grid. Therefore some countries have issued dedicated grid codes for connecting the wind turbines to the grid. A detailed review of international grid code requirements is presented in [14], [15] and [16].

In most of the cases, these grid code requirements have focus on power quality, power controllability and fault ride-through capability. Moreover, in some grid codes requirement for ancillary services are stated during a network disturbance, the WECS control has to regulate the supply reactive power to the electrical grid. The most demanding requirements regarding the controllability of the produced power are specified in the Danish grid code, which demands to the wind turbines behaviour similar to conventional power plant, i.e. WECSs have to be part of primary and secondary control systems.

A main concern is the LVRT capability of grid connected wind turbines due to voltage sags, which are the most prevalent disturbances in electrical power system. According with recent surveys, grid-voltage sags represent 92% of all disturbances into the electrical grid [17]. Moreover, 88% of voltage sags are asymmetrical [18].

All existing grid codes require fault ride-through capabilities for wind turbines. Voltage profiles are given specifying the depth of the voltage dip and the clearance time as well. Fig. 5 shows the LVRT requirements from different national grid codes when symmetrical grid-voltage sags appears [15], [19] and [20].

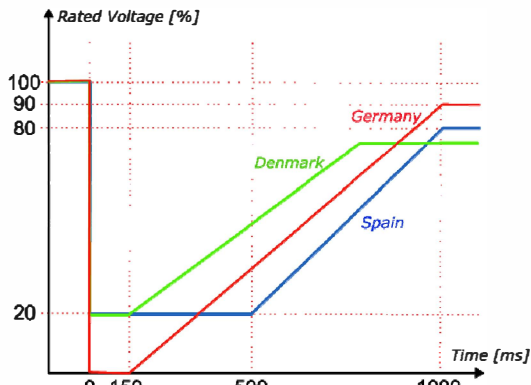


Figure 5: LVRT requirements. Voltage profile for simulation of symmetric three-phase faults in Germany, Denmark and Spain

System Operators demand to wind farm provide a report detailing the simulation model and results for the voltage

profile given in Fig.6. The WECSs must stay connected for grid-voltage sags when the grid voltage is within specified boundaries.

In Fig. 6 the requirement for reactive power is shown. During the voltage dip the reactive power control must be changed from normal operation –typically unitary power factor– to a maximum voltage support strategy. If it is required, the WECS must be able to provide full rated reactive power to help to re-establish the normal grid voltage as soon as possible.

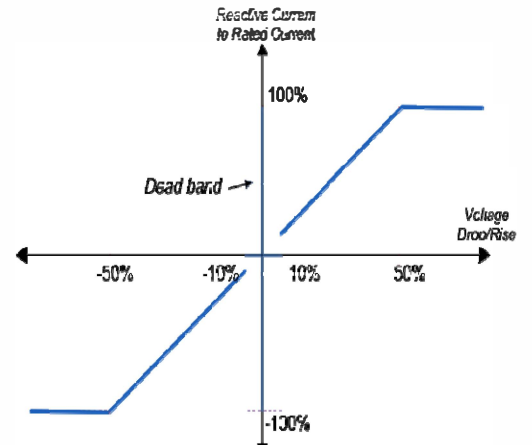


Figure 6: LVRT requirements. Reactive power requirement as a function of the grid voltage for the Spanish grid code.

V. PROPOSED CONTROL STRATEGY FOR THE M3C

A. Published Control Strategies

The application of M3C to drive high power WECS have been barely investigated. Actually, very few publications have reported experimental implementations for this topology driving electrical machines. However, some cascaded control strategies have been proposed in [9], [10], [11], [12] and [13]. In [9] and [10], the strategies are based in the injection of positive and negative sequence input current to perform average and energy balancing of the cell capacitors. On the other hand, fully decoupled models are obtained in [11] and [12] for the control of the M3C. In these papers, the input current control, the energy balancing control and the output current control are completely decoupled.

All the cited control strategies consider a cascade control, with an inner loop for branch currents regulation and an outer control loop for energy balancing of cell capacitors. Mainly, these control schemes are based on Proportional controllers for the internal balancing currents and Proportional-Integral regulators to handle the input and output currents and to perform average energy balancing.

Nowadays, to the best of the authors knowledge, research works regarding the use of the M3C in high power wind energy applications have not been reported in recent literature.

B. Proposed Control Strategy

The proposed control strategy is based in the model presented in (9)-(11), which allows fully decoupled regulation of

the input, circulating and output currents. Fig. 8 shows the overview of the

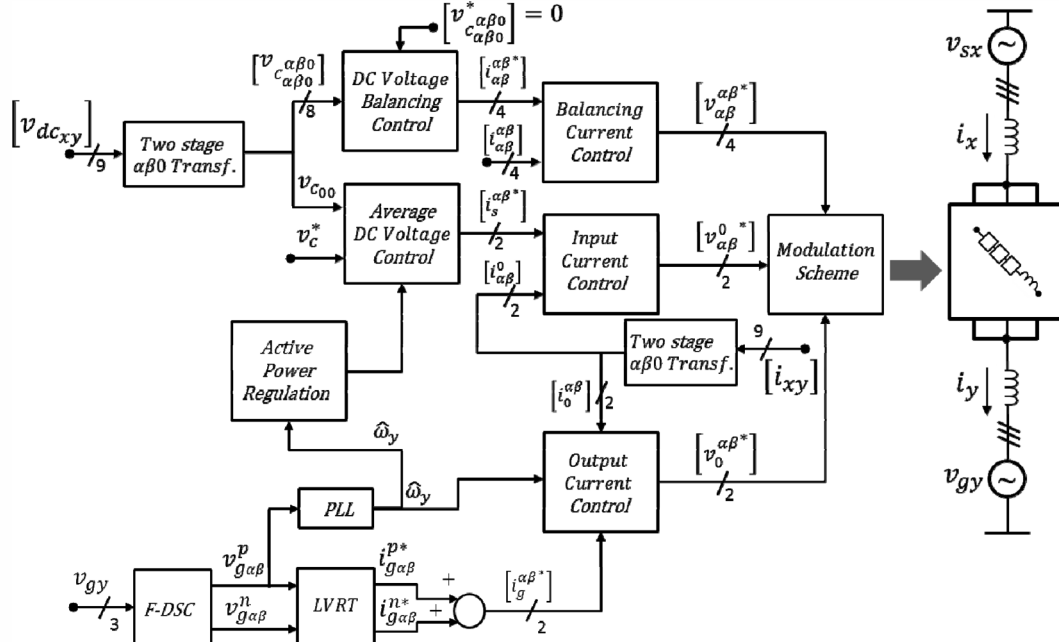


Fig. 8: Overview of the proposed control strategy.

proposed control strategy for M3C based High-Power WECS fulfilling LVRT requirements, which can be structured on the following subcontrols modules:

1) Voltage control of DC Capacitors

The Total Energy stored in the capacitor of one branch can be expressed as:

$$W_{xy} = \int P_{xy} dt = \frac{nC}{2} \bar{v}_c^2 \rightarrow P_{xy} = nC \bar{v}_c \frac{d}{dt}(\bar{v}_c) \rightarrow \frac{d}{dt}(\bar{v}_c) = \frac{1}{nC\bar{v}_c} P_{xy} \quad (12)$$

where P_{xy} represents the branch power, v_c represents the dc capacitors average voltage, n is number of cells, C represents the capacitance of each capacitor and W_{xy} symbolizes the total energy in the n dc capacitors. Considering the whole converter, it is possible to write:

$$\begin{bmatrix} v_{c_{ar}} & v_{c_{as}} & v_{c_{at}} \\ v_{c_{br}} & v_{c_{bs}} & v_{c_{bt}} \\ v_{c_{cr}} & v_{c_{cs}} & v_{c_{ct}} \end{bmatrix} = \frac{1}{nC\bar{v}_c^0} \int \begin{bmatrix} P_{ar} & P_{as} & P_{at} \\ P_{br} & P_{bs} & P_{bt} \\ P_{cr} & P_{cs} & P_{ct} \end{bmatrix} dt + \bar{v}_c^0 \begin{bmatrix} 1 & 1 & 1 \\ 1 & 1 & 1 \\ 1 & 1 & 1 \end{bmatrix} \quad (13)$$

The two stages $\alpha\beta 0$ transformation presented in Fig. 4 implies the transformation of (13) in:

$$\begin{bmatrix} v_{c_{\alpha\alpha}} & v_{c_{\beta\alpha}} & v_{c_{0\alpha}} \\ v_{c_{\alpha\beta}} & v_{c_{\beta\beta}} & v_{c_{0\beta}} \\ v_{c_{\alpha 0}} & v_{c_{\beta 0}} & v_{c_{00}} \end{bmatrix} = \frac{1}{3nC\bar{v}_c^0} \int \begin{bmatrix} P_{\alpha\alpha} & P_{\beta\alpha} & P_{0\alpha} \\ P_{\alpha\beta} & P_{\beta\beta} & P_{0\beta} \\ P_{\alpha 0} & P_{\beta 0} & P_{00} \end{bmatrix} dt + \begin{bmatrix} 0 & 0 & 0 \\ 0 & 0 & 0 \\ 0 & 0 & 3\bar{v}_c \end{bmatrix} \quad (14)$$

In (13) and (14) the nine power elements are related to the nine capacitor voltages. This fact suggests that is correct to use energy balancing to keep proper regulation of the dc voltage capacitors.

Average control

The component $v_{c_{00}}$ is related to the average value of all capacitor voltages \bar{v}_c , which can be controlled using the active power flowing into the converter P_{00} . This is the basis for the average dc voltage capacitors control, which generates the input current reference $i_s^{\alpha\beta*}$, using PI controllers, as is shown in Fig. 8. In fact, when all the elements of the matrix $[v_{c_{xy}}]$ are equal to \bar{v}_{dc}^* , the dc voltage capacitor references can be calculated as is depicted in (24) and just the average control reference is obtained.

$$\begin{bmatrix} v_{c_{\alpha\alpha}}^* & v_{c_{\beta\alpha}}^* & v_{c_{0\alpha}}^* \\ v_{c_{\alpha\beta}}^* & v_{c_{\beta\beta}}^* & v_{c_{0\beta}}^* \\ v_{c_{\alpha 0}}^* & v_{c_{\beta 0}}^* & v_{c_{00}}^* \end{bmatrix} = \begin{bmatrix} 0 & 0 & 0 \\ 0 & 0 & 0 \\ 0 & 0 & 3\bar{v}_{dc}^* \end{bmatrix} \quad (15)$$

Balancing control

The other eight components of (14) represent the power between one subconverter and another –usually named horizontal balancing– or between different branches in the same subconverter, which is called vertical balancing. The oscillating power components should be to zero in order to mitigate the ripple in the dc capacitor voltages. As is presented in [12], the eight power components can be regulated by

controlling the four circulating currents $\begin{bmatrix} i_{\alpha\beta}^{\alpha\beta} \end{bmatrix}$. Therefore, a cascade control is utilised in order to provide an outer power loop to generate the references $\begin{bmatrix} i_{\alpha\beta}^{\alpha\beta*} \end{bmatrix}$.

2) Input current control:

When $\alpha\beta$ reference frame is used to control the system, the use of a resonant controller commonly preferred [21], [22]. Considering (9), a simple Resonant Regulator could be used in order to control the input currents as follow:

$$\begin{bmatrix} v_{\alpha 0}^* \\ v_{\beta 0}^* \end{bmatrix} = \begin{bmatrix} v_{s\alpha} \\ v_{s\beta} \end{bmatrix} - (L_1 + \frac{L_2}{3}) \frac{d}{dt} \begin{bmatrix} i_{s\alpha} \\ i_{s\beta} \end{bmatrix} + C_{RC}(s) \begin{bmatrix} i_{s\alpha}^* - i_{s\alpha} \\ i_{s\beta}^* - i_{s\beta} \end{bmatrix} \quad (16)$$

Where $i_{s\alpha}^*$ and $i_{s\beta}^*$ are regulated using the average DC voltage control. Furthermore, using superposition this control scheme can be easily linked with a frequency support control loop using, for example, Inertia Emulation or Droop Control [23].

3) Circulating current control

Due to the topology of the converter, the branch currents, and consequently circulating currents, contain different frequency components (rotating at ω_x and ω_y). Proportional controllers could be well suited for this application, but do not ensure zero error in steady state if perturbation are incorporated to the system. On the other hand, PI and Resonant controllers should be tuned to the different frequencies in order to achieve proper operation, which lead to an increment of the control design complexity. Other linear controllers could be a solution more simple, like Dead-Beat controllers [9], which are used in this application.

According with (10), the voltage commands to achieve decoupled current control of the four circulating currents should be:

$$\begin{bmatrix} v_{\alpha\alpha}^* & v_{\beta\alpha}^* \\ v_{\alpha\beta}^* & v_{\beta\beta}^* \end{bmatrix} = -C_{DB}(s) \left(\begin{bmatrix} i_{\alpha\alpha}^* & i_{\beta\alpha}^* \\ i_{\alpha\beta}^* & i_{\beta\beta}^* \end{bmatrix} - \begin{bmatrix} i_{\alpha\alpha} & i_{\beta\alpha} \\ i_{\alpha\beta} & i_{\beta\beta} \end{bmatrix} \right) \quad (17)$$

4) Output current control

The apparent power at grid terminal, calculated considering three-leg unbalanced system with positive -and negative- sequence components, is show in (18):

$$\bar{S}_g = \left(\bar{v}_{g\alpha\beta}^p + \bar{v}_{g\alpha\beta}^n \right) \left(\bar{i}_{g\alpha\beta}^p + \bar{i}_{g\alpha\beta}^n \right)^c \quad (18)$$

The superscripts (c), (p), and (n) are used to denote the complex conjugate of the current vector, positive-sequence component and negative-sequence component, respectively. Expanding (18) and separating real and imaginary parts:

$$P_g = P_{g0} + P_{gc2} \cos 2\omega t + P_{gs2} \sin 2\omega t \quad (19)$$

$$Q_g = Q_{g0} + Q_{gc2} \cos 2\omega t + Q_{gs2} \sin 2\omega t \quad (20)$$

According to [24], (19) and (20) could be expressed in stationary reference frame as follow:

$$\begin{bmatrix} i_{g\alpha}^p \\ i_{g\beta}^p \\ i_{g\alpha}^n \\ i_{g\beta}^n \end{bmatrix} = \begin{bmatrix} v_{g\alpha}^p & v_{g\beta}^p & v_{g\alpha}^n & v_{g\beta}^n \\ v_{g\beta}^p & -v_{g\alpha}^p & v_{g\beta}^n & -v_{g\alpha}^n \\ v_{g\alpha}^n & -v_{g\beta}^n & -v_{g\alpha}^p & v_{g\beta}^p \\ v_{g\alpha}^p & v_{g\beta}^p & v_{g\alpha}^n & v_{g\beta}^n \end{bmatrix}^{-1} \begin{bmatrix} P_{g0} \\ Q_{g0} \\ P_{fs2} \\ P_{fc2} \end{bmatrix} \quad (21)$$

In order to regulate the power injected to the electrical network, positive and negative sequence currents have to be controlled. As is shown in (21), to obtain these currents the positive and negative grid-voltage components are required. Therefore, a separation sequence method is required to guarantees the identification of the positive and negative sequence components. Moreover, correct grid frequency detection is ensured when a separation sequence method is utilised [25].

Delayed-signal-cancellation (DSC) is probably the best suited method, but presents an intrinsic delay of $T/4$. To reduce the intrinsic delay present in DSC, in [26] a fast convergence DSC is proposed, using the following expressions:

$$\bar{v}_{g\alpha\beta}^p = \frac{\bar{v}_{g\alpha\beta}(\omega t) - e^{-j\theta_d} \bar{v}_{g\alpha\beta}(\omega t - \theta_d)}{1 - e^{-j2\theta_d}} \quad (19)$$

$$\bar{v}_{g\alpha\beta}^n = \frac{\bar{v}_{g\alpha\beta}(\omega t) - e^{-j\theta_d} \bar{v}_{g\alpha\beta}(\omega t - \theta_d)}{1 - e^{j2\theta_d}} \quad (20)$$

where θ_d is the delay angle. In an experimental implementation, this angle is calculated as $\theta_d = 2\pi T / (NT_s)$ where N is an integer. Therefore, the separation method depicted in (19)-(20) is utilised in this work to obtain the positive and negative sequence components of the grid voltage and calculate (21).

Due to Resonant controllers (RC) can be used to regulate positive and negative sequence current at the same time, are used in the output current control. Actually, only two RC are needed instead of four for d-q axis based control systems [27]. Additionally, for LVRT control, orientation along any of the voltage or current vectors is not required and a PLL is implemented only to obtain the grid-frequency, which is used to tune the RC.

At this point, voltage commands to achieve decoupled output current control using RC can be obtained as follow:

$$\begin{bmatrix} v_{\alpha}^* \\ v_{\beta}^* \end{bmatrix} = \begin{bmatrix} v_{g\alpha} \\ v_{g\beta} \end{bmatrix} - (L_1 + \frac{L_2}{3}) \frac{d}{dt} \begin{bmatrix} i_{g\alpha} \\ i_{g\beta} \end{bmatrix} - C_{RC}(s) \begin{bmatrix} (i_{g\alpha}^{p*} + i_{g\alpha}^{n*}) - i_{s\alpha} \\ (i_{g\beta}^{p*} + i_{g\beta}^{n*}) - i_{s\beta} \end{bmatrix} \quad (18)$$

VI. RESULTS

This section presents simulation results for the system shown in Fig.2. The system has been testes under grid-voltage dips in order to validate the novel application of M3C driving high-power grid-connected WECS.

A simulation model for a three cells per branch M3C has been development using PLECS software. The general parameters are depicted in Table I.

Table I: Simulation Parameters

Rated Active Power	50 kW
Cells per branch	3
Input Voltage	690 V

Input frequency	10-40 Hz
Input inductor	3mH
Branch Inductor	2.5 mH
Capacitance in each cell	5mF
DC-Capacitor Voltage	600 V
RL Load	$R=6\Omega$ and $L=2.5\text{mH}$.

Output frequency	50 Hz
Output voltage	690 V
Output inductor	3mH
Switching frequency	2kHz

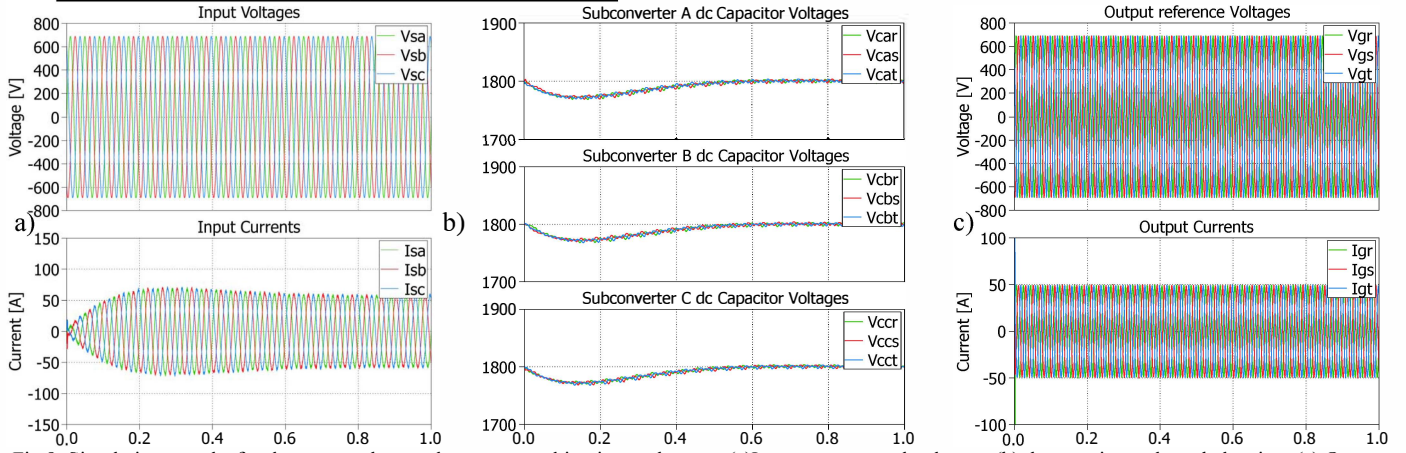


Fig 9. Simulations results for the proposed control strategy working in steady state. (a) Input currents and voltages. (b) dc capacitor voltage balancing. (c) Output currents and voltages fed to the grid.

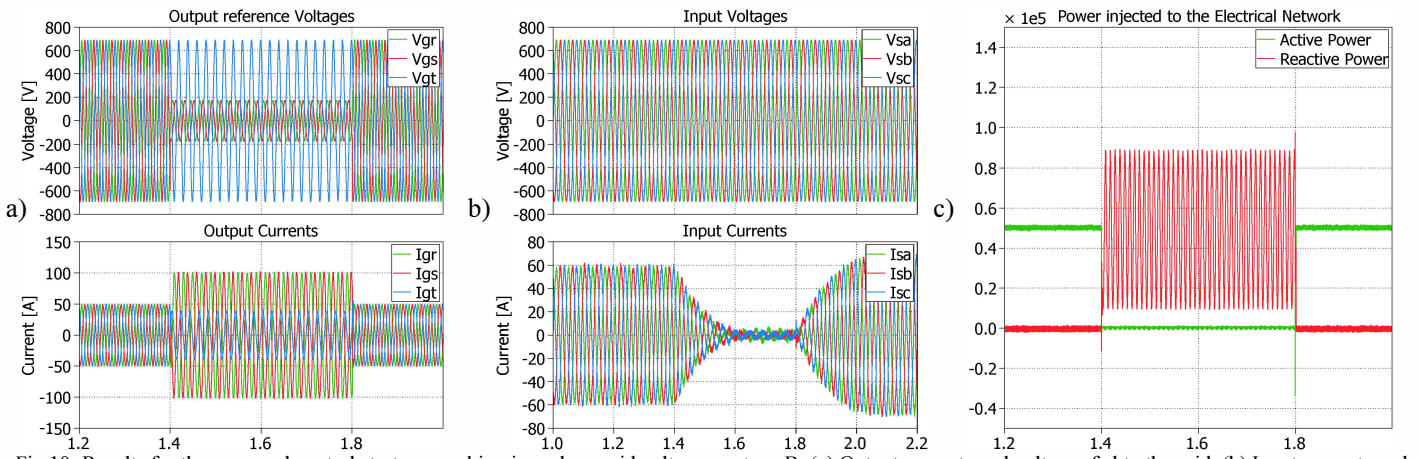


Fig 10: Results for the proposed control strategy working in under a grid voltage sag type B. (a) Output currents and voltages fed to the grid. (b) Input currents and voltages. (c) Active and Reactive Power injected to the electrical network

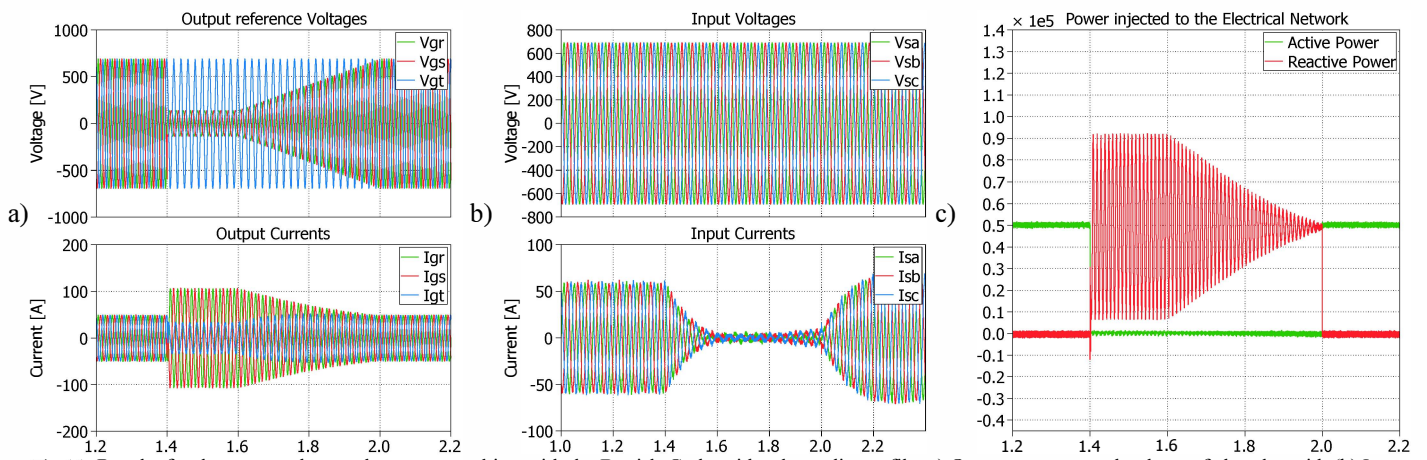


Fig 11. Results for the proposed control strategy working with the Danish-Code grid-voltage dip profile. (a) Output currents and voltages fed to the grid. (b) Input currents and voltages. (c) Active and Reactive Power injected to the electrical network.

The simulation parameters are chosen in order to achieve the best approximation to the experimental setup expected to be built in the near future. However, experimental validations are out of the scope of this paper

The application of the M3C under steady state is presented in Fig. 9. As can be observed, the proposed control strategy allows proper operation of the converter keeping regulation of the dc capacitor voltages, input current and voltages and output current and voltages.

Additionally, tests to check LVRT capabilities have been carried out. The first test consists in operating the system under a grid-voltage type C. As is shown in Fig. 10(a), the fault is introduced in $t=1.4$ s and cleared in $t=1.8$ s. When the fault appears, the input current control stops the active power generation by reducing the current to zero (Fig. 10(b)). The output currents are controlled using the calculation presented in (21), which generates unbalanced references in order to mitigate the effects of the grid voltage dip. At the fault time appearance, the active power injected to the grid is 0-kW in order to support the grid voltage through full reactive power injection, as is shown in Fig. 10(c). There is not presence of double-frequency oscillations in active power, but reactive power presents double frequency oscillations that cannot be controlled in any case because there are not enough degrees of freedom [19], [27].

The second LVRT test introduces a grid voltage dip based on the regulations present in the Danish grid code, [15], [19].

The voltage profile is presented in Fig. 11(a). When the fault starts, the input current control stops the input active power generation –as is shown in Fig. 11(b)– because the active power injected to the grid is regulated to zero. The active and reactive power waveforms are presented in Fig. 11(c).

For both LVRT tests, the dc capacitor voltages are illustrated in Fig. 11. It is possible to observe that the proposed control strategy really decouples the converter, allowing independent control for the input, output and circulating current. Therefore, proper energy balancing is achieved when grid voltage faults occur. When the faults appear, a slightly voltage increase can be observed. This is produced because the output power control has a faster dynamic response than the input current control, which needs almost 200ms to reduce the input current to zero. Nonetheless, it can be observed in Fig. 11 that the dc capacitor voltage is not affected when a grid voltage appears in the point of common connection between the M3C and the electrical network.

Finally, an increase in the dc capacitor average voltage is introduced in $t=2.4$ s, changing the reference in each cell from 600V to 667V. It can be seen in Fig. 12 that the output currents and voltages are not affected during the change of reference. In fact, the average control of the dc voltage control just requires an increase in the input current to reach the new reference level.

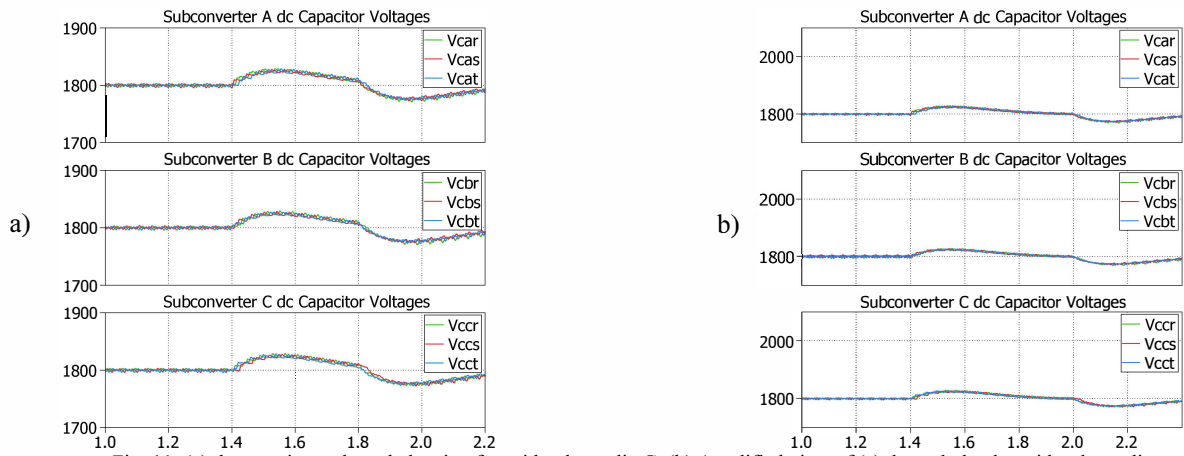


Fig. 11: (a) dc capacitor voltage balancing for grid voltage dip C. (b) Amplified view of (a) through the the grid-voltage dip.

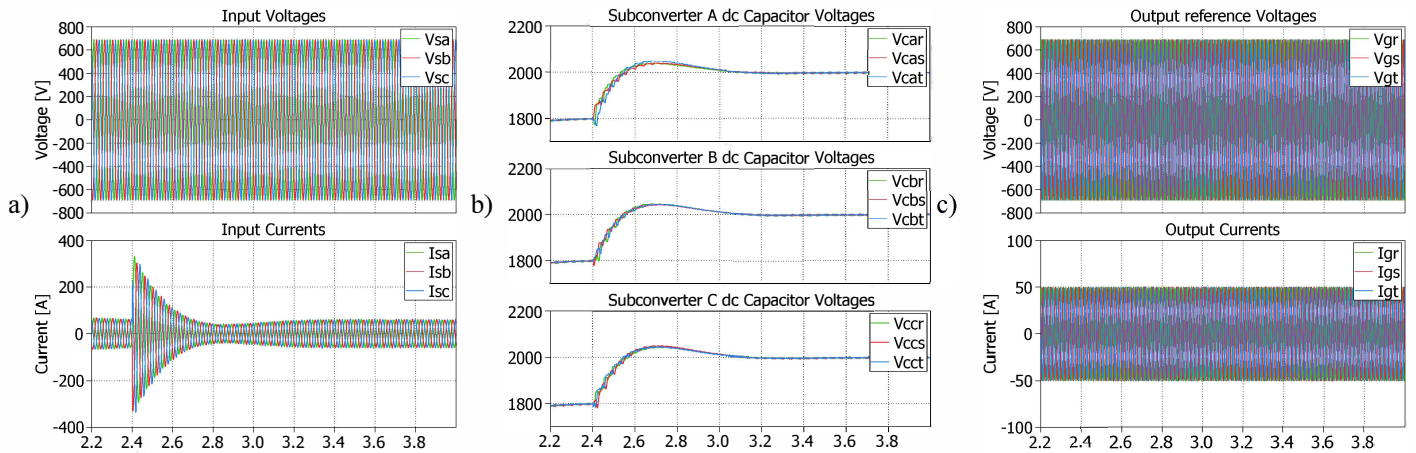


Fig 12. Simulations results for the proposed control strategy under and increment in the average dc capacitor voltages. (a) Input currents and voltages. (b) dc capacitor voltage balancing. (c) Output currents and voltages fed to the grid.

VII. CONCLUSIONS

A fully decoupled control strategy for the application of the Modular Multilevel Matrix Converter in high-power WECS has been proposed in this paper. Beyond the current state of the art, WECS based on the Modular Multilevel Matrix Converter are a novel concept that could be applied successfully in wind turbines up to 20MW, as is demonstrate in this preliminary work.

The proposed decoupled control allows independent current and energy balancing regulation. Furthermore, the two-stage $\alpha\beta 0$ transformation allows the identification of three independent systems, which are used to control the input currents, the output currents and the internal circulating currents.

Four circulating currents are obtained from the nine branch currents by applying the two-stage $\alpha\beta 0$ transformation. These circulating currents are used to perform energy balancing keeping the dc voltages regulated independently of the input/output conditions.

The proposed control strategy has been validate through simulations obtained from a 50 kW M3C based WECS. Results show that the proposed control strategy meets the LVRT requirements as well proper energy balancing is performed. Accordingly, the strategy is able to keep the system grid-connected through grid-voltage dip conditions, as the presented in Fig. 10 and Fig. 11. Moreover, the system is able to support grid-voltage through reactive power injection.

VIII. AKNOLOGMENTS

The authors would like to thank the support provided by the Chilean National Fund of Scientific and Technological Development (FONDECYT) grant Nr. 1140337 and the Advanced Centre for Electrical and Electronic Engineering, AC3E, Basal Project FB0008

IX. REFERENCES

- [1] Danish Commission Climate Change Policy, "Green Energy—The Road to a Danish Energy System Without Fossil Fuels," 2010.
- [2] EWEA, "Upwind: Design limits and solutions for very large wind turbines."
- [3] S. Kouro, M. Malinowski, K. Gopakumar, J. Pou, L. G. Franquelo, J. Rodriguez, M. A. Pérez, and J. I. Leon, "Recent Advances and Industrial Applications of Multilevel Converters," *IEEE Trans. Ind. Electron.*, vol. 57, no. 8, pp. 2553–2580, Aug. 2010.
- [4] L. Franquelo, J. Rodriguez, J. Leon, S. Kouro, R. Portillo, and M. Prats, "The age of multilevel converters arrives," *IEEE Ind. Electron. Mag.*, vol. 2, no. 2, pp. 28–39, Jun. 2008.
- [5] R. W. Erickson and O. A. Al-Naseem, "A new family of matrix converters," in *IECON'01. 27th Annual Conference of the IEEE Industrial Electronics Society (Cat. No.37243)*, 2001, vol. 2, pp. 1515–1520.
- [6] S. Angkititrakul and R. W. Erickson, "Control and implementation of a new modular matrix converter," in *Nineteenth Annual IEEE Applied Power Electronics Conference and Exposition, 2004. APEC '04.*, 2004, vol. 2, pp. 813–819.
- [7] S. Angkititrakul and R. W. Erickson, "Capacitor Voltage Balancing Control for a Modular Matrix Converter," in *Twenty-First Annual IEEE Applied Power Electronics Conference and Exposition, 2006. APEC '06.*, 2006, pp. 1659–1665.
- [8] A. Korn, M. Winkelkemper, P. Steimer, and J. W. Kolar, "Direct modular multi-level converter for gearless low-speed drives." pp. 1–7, 2011.
- [9] J. Borquez, "Control de un Conversor Matricial Multinivel Tipo Cascada," University of Magallanes, 2010.
- [10] F. Kammerer, J. Kolb, and M. Braun, "A novel cascaded vector control scheme for the Modular

- Multilevel Matrix Converter,” in *IECON 2011 - 37th Annual Conference of the IEEE Industrial Electronics Society*, 2011, pp. 1097–1102.
- [11] F. Kammerer, J. Kolb, and M. Braun, “Fully decoupled current control and energy balancing of the Modular Multilevel Matrix Converter,” in *2012 15th International Power Electronics and Motion Control Conference (EPE/PEMC)*, 2012, pp. LS2a.3–1–LS2a.3–8.
- [12] W. Kawamura, M. Hagiwara, and H. Akagi, “Control and experiment of a 380-V, 15-kW motor drive using modular multilevel cascade converter based on triple-star bridge cells (MMCC-TSBC),” in *2014 International Power Electronics Conference (IPEC-Hiroshima 2014 - ECCE ASIA)*, 2014, pp. 3742–3749.
- [13] W. Kawamura, M. Hagiwara, and H. Akagi, “Control and Experiment of a Modular Multilevel Cascade Converter Based on Triple-Star Bridge Cells,” *IEEE Trans. Ind. Appl.*, vol. 50, no. 5, pp. 3536–3548, Sep. 2014.
- [14] M. Altn, O. Goksu, R. Teodorescu, P. Rodriguez, B.-B. Jensen, and L. Helle, “Overview of recent grid codes for wind power integration,” *Optimization of Electrical and Electronic Equipment (OPTIM)*, 2010 12th International Conference on. pp. 1152–1160, 2010.
- [15] M. Altn, O. Goksu, R. Teodorescu, P. Rodriguez, B.-B. Jensen, and L. Helle, “Overview of recent grid codes for wind power integration,” *Optimization of Electrical and Electronic Equipment (OPTIM)*, 2010 12th International Conference on. pp. 1152–1160, 2010.
- [16] N. C. F. Iov, A. Hansen, P. Sørensen, “Mapping of grid faults and grid codes,” *Risø-R-1617(EN)* 41 p.
- [17] O. S. Senturk and A. M. Hava, “A simple sag generator using SSRs,” in *2010 IEEE Energy Conversion Congress and Exposition*, 2010, pp. 4049–4056.
- [18] R. Cárdenas, R. Peña, S. Alepuz, and G. Asher, “Overview of Control Systems for the Operation of DFIGs in Wind Energy Applications,” *IEEE Trans. Ind. Electron.*, vol. 60, no. 7, pp. 2776–2798, 2013.
- [19] S. Alepuz, S. Busquets-Monge, J. Bordonau, J. A. Martinez-Velasco, C. A. Silva, J. Pontt, and J. Rodriguez, “Control Strategies Based on Symmetrical Components for Grid-Connected Converters Under Voltage Dips,” *IEEE Trans. Ind. Electron.*, vol. 56, no. 6, pp. 2162–2173, Jun. 2009.
- [20] M. Tsili and S. Papathanassiou, “A review of grid code technical requirements for wind farms,” *IET Renew. Power Gener.*, vol. 3, no. 3, p. 308, 2009.
- [21] M. Diaz and R. Cardenas, “The application of resonant controller to fulfill LVRT requirements in grid connected VSI,” in *2013 Eighth International Conference and Exhibition on Ecological Vehicles and Renewable Energies (EVER)*, 2013, pp. 1–8.
- [22] R. Cardenas, C. Juri, R. Pena, J. Clare, and P. Wheeler, “Analysis and Experimental Validation of Control Systems for Four-Leg Matrix Converter Applications,” *IEEE Trans. Ind. Electron.*, vol. 59, no. 1, pp. 141–153, Jan. 2012.
- [23] M. Liserre, R. Cardenas, M. Molinas, and J. Rodriguez, “Overview of Multi-MW Wind Turbines and Wind Parks,” *IEEE Trans. Ind. Electron.*, vol. 58, no. 4, pp. 1081–1095, Apr. 2011.
- [24] M. Diaz and R. Cardenas, “The application of resonant controller to fulfill LVRT requirements in grid connected VSI,” in *2013 Eighth International Conference and Exhibition on Ecological Vehicles and Renewable Energies (EVER)*, 2013, pp. 1–8.
- [25] P. Rodriguez, J. Pou, J. Bergas, I. Candela, R. Burgos, and D. Boroyevic, “Double Synchronous Reference Frame PLL for Power Converters Control,” in *IEEE 36th Conference on Power Electronics Specialists, 2005.*, 2005, pp. 1415–1421.
- [26] R. Cardenas, M. Díaz, F. Rojas, and J. Clare, “Fast Delayed Signal Cancellation Method for Component Sequences Separation,” *IEEE Power Eng. Lett.*, no. Submitted.
- [27] M. Diaz and R. Cardenas, “Analysis of synchronous and stationary reference frame control strategies to fulfill LVRT requirements in Wind Energy Conversion Systems,” in *2014 Ninth International Conference on Ecological Vehicles and Renewable Energies (EVER)*, 2014, pp. 1–8.

